Characteristic Analysis and Comparison of IPMSM for HEV According to Pole and Slot Combination

Jae-Woo Jung[1], Jung-Pyo Hong[1], *Senior Member*, *IEEE*, and Young-Kyoun Kim[2]
[1]Department of Automotive Engineering, Hanyang University, Seoul, 133-791, Korea
jjw@hanyang.ac.kr, hongjp@hanyang.ac.kr
[2]Artificial Intelligent & Mechatronics Research Center, Korea Electronics Technology Institute, Puchon, 420-140, Korea

***Abstract*- Interior permanent magnet synchronous motor (IPMSM) is usually applied to traction motor in the hybrid electric vehicle (HEV). All motors including IPMSM have different parameters and characteristics with various combinations of the number of poles and slots. The proper combination can improve characteristics of traction system ultimately. This paper deals with analysis of the characteristics of IPMSM for mild type HEV according to the combinations of number of poles and slots. The specific models with 16-pole/18-slot, 16-pole/24-slot and 12-pole/18-slot combinations are introduced. And the advantages and disadvantages of these three models are compared. The characteristics of each model are computed in d-q axis equivalent circuit analysis and finite element analysis. After then, the proper combination of the number of poles and slots for HEV traction motor is presented after comparing these three models.**

I. INTRODUCTION

The alternative energy source and high efficiency electric machine is researched as a part of effort to reduce air pollution and global warming caused by automobile exhausts. Hybrid electric vehicle (HEV), Fuel cell electric vehicle (FCEV) and Electric vehicle (EV) is studied by many researchers especially in the automotive field. FCEV and EV that is operated with electric energy are limited by performance of battery and fuel cell. Therefore HEV is expected alternative solution in the long term. The main technique of HEV reduces the emission by using both engine and traction motor [1]. In order to increase fuel efficiency, optimal control strategy is required according to operating condition of vehicle. However beyond of optimal control, performance for traction motor should be maximized.

In the motor, there are different parameters and characteristics such as winding factor, d- and q-axis inductance, saliency ratio and force etc, which depend on the combination of the number of poles and slots. Therefore, the combination of the number of pole and slot number is determined carefully in the initial design process to achieve high performance. In this paper, characteristic analysis of interior permanent magnet synchronous motor (IPMSM) is used to investigate the performance of HEV traction motor. Comparison analysis is performed according to various combination of the number of poles and slots using d-q axis equivalent circuit analysis and finite element method (FEM). Based on the comparison result, the suitable combination for the HEV traction motor is presented.

II. ANALYSIS MODEL

A. *Specification of analysis model*

The analysis model is IPMSM which is applied in traction motor for mild type HEV. The specification of the IPMSM is shown in Table I. The battery voltage is 155V and R.M.S. value of current is 200A as constraint condition. The maximum torque, 105Nm is produced by maximum torque per ampere (MTPA) control at the low speed, from 0 to 1200rpm. Flux weakening control is applied to expand speed range and keep the constant power.

B. *Combination of the number of pole and slot*

The combination of the number of pole and slot is important factor which should be determined in the initial design processor. First of all, the back-EMF is most important parameter that affects the output power and performance in the motor. Assume that same number of conductor and area of cross section of permanent magnet in the motor, the back-EMF is varied according to each combination of the number of poles and slots. The IPMSM which is studied in this paper is limited with 12 and 16 pole to be easy to select a resolver. The 12-pole/18-slot, 16-pole/18-slot, and 16-pole/24-slot combinations are considered. These winding distributions are symmetry and have large winding factor as shown in Table II.

TABLE I
SPECIFICATION OF ANALYSIS MODEL

Item	Value	Unit	Remark
Input voltage	155	V_{dc}	DC link
Max. torque	105	Nm	-
Output power	15	kW	Max.
Current limit	200	A_{rms}	Max.
Base speed	2000	rpm	MTPA
Max. speed	6000	rpm	Flux weakening

TABLE II
WINDING FACTOR ACCORDING TO COMBINATION OF THE NUMBER OF POLE AND SLOT NUMBER

Slot \ Pole	4	6	8	10	12	14	16
6	0.866		0.866	0.500		0.500	0.866
9	0.617	0.866	0.945	0.945	0.866	0.617	0.328
12			0.866	0.933		0.933	0.866
15			0.711	0.866		0.951	0.951
18				0.735	0.866	0.901	0.945
21						0.866	0.891
24						0.760	0.866

C. *Configuration of analysis model*

The configuration and structure of analysis model which is shown in Fig. 1 and it shows single electrical period of the full model. The wining distribution of 16-pole/18-slot model is different to the others. The winding of one phase is concentrated spatially. This winding structure creates inequality magnetic force distribution in the air gap and this effect will be considered in this paper.

It is hard to design the rotor with 'V-shape' of permanent magnet (PM) in the 12-pole/18-slot model due to constrain condition as shown in Fig.1 (c). Therefore the structure of PM is designed to '- shape' in 12-pole/18-slot model.

III. PARAMETERS OF ANALYSIS MODEL

In order to design the motor, parameter such as back-EMF and inductance should be calculated exactly. The parameter of motor is computed by numerical analysis.

A. *Noload back-EMF*

The back-EMF of the each model is calculated using FEM. The result of back-EMF and harmonic analysis is shown in Fig. 2 (a) and Fig. 2 (b), (c), (d) respectively. Total harmonic distortion (THD) of back-EMF with 16-pole/18-slot model is lowest as shown Table III because of unusual winding distribution. Fig. 3 shows the principle of back-EMF generation in the 16-pole/18-slot model. Assume that the rotor is rotated with counter clock wise with N, S pole as shown in Fig. 3 (a), back-EMF which is generated each slot winding has phase difference. Fig. 3 (c) shows vector sum of back-EMF each parallel. It is same with skew effect. This is why the back-EMF of 16-pole/18-slot model shows better sinusoidal shape than the other models.

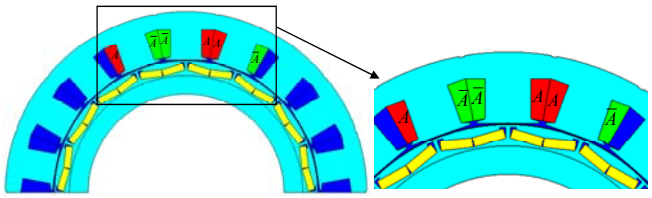

(a) 16-pole/18-slot model

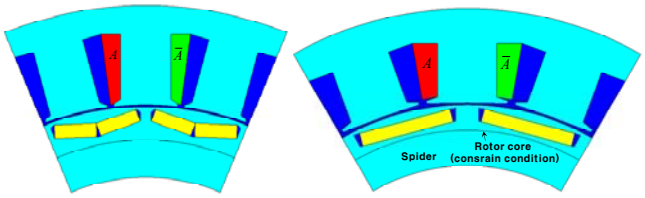

(b) 16-pole/24-slot model (c) 12-pole/18-slot model

Fig. 1. Configuration and structure of analysis models

TABLE III
THD OF BACK-EMF

Model	16-pole/18-slot	16-pole/24-slot	12-pole/18-slot
THD [%]	0.1	5.5	4.2

However, if stator winding is connected parallel circuit, there is voltage difference, 20° electrical angle among the three parallel winding as follow (1). It causes that 16-pole/18-slot model has circulation current when it is operated no-load condition. It is the reason why the thermal rising of stator coil in 16-pole/18-slot model is higher than in the others.

$$\begin{aligned} e_{A1,A4} &= e\cos(\omega t - 0) \\ e_{A2,A5} &= e\cos(\omega t - 20) \\ e_{A3,A6} &= e\cos(\omega t - 40) \end{aligned} \tag{1}$$

where $e_{A1,A4}$, e_{A2A5}, e_{A3A6}: back-EMF produced each parallel circuit.

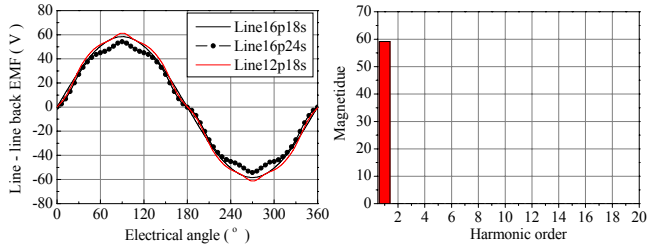

(a) Back-EMF (b) Harmonics of 16-pole/18-slot

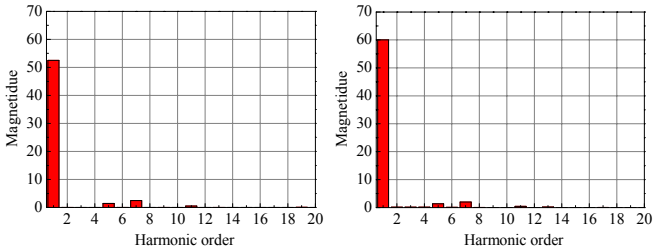

(c) Harmonics of 16-pole/24-slot (c) Harmonics of 12-pole/18-slot

Fig. 2. Result of back-EMF each models

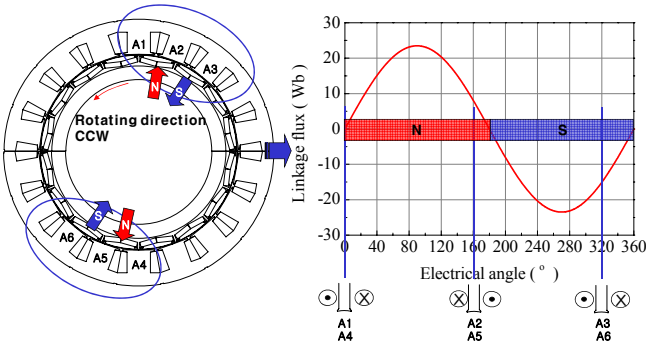

(a) Relationship between winding and linkage flux

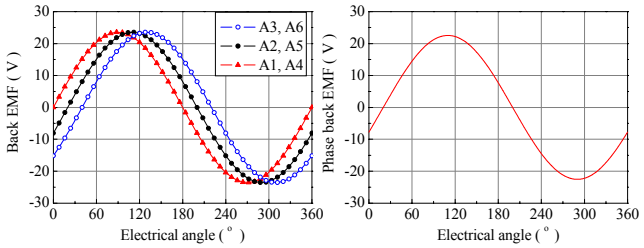

(b) Back-EMF of each position (c) Phase back-EMF

Fig. 3. Principle of back-EMF generation in 16-pole/18-slot model

B. *Inductance profile*

Inductance profile is calculated according to current and current angle. The vector diagram is presented in Fig. 4 in order to explain calculation of d- and q-axis inductance profile. The d- and q-axis inductance profile is calculated using the relation between flux linkage of noload and load condition as shown in (2) and (3) [2]. Finite element analysis is employed to compute linkage flux. Fig. 5 shows d- and q-axis inductance profile according to current and current angle for 16-pole/24-slot model. The aspects of d- and q-axis inductance profiles of other combinations are similar.

$$L_d = \frac{\psi_0 \cos\alpha - \psi_a}{i_d}, \quad L_q = \frac{\psi_0 \sin\alpha}{i_q} \tag{2}$$

$$i_d = -I_a \sin\beta, \quad i_q = I_a \cos\beta \tag{3}$$

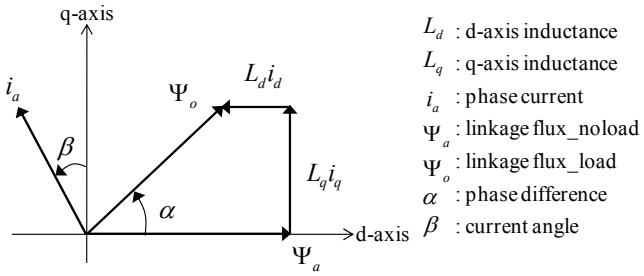

Fig. 4. Vector diagram of IPMSM

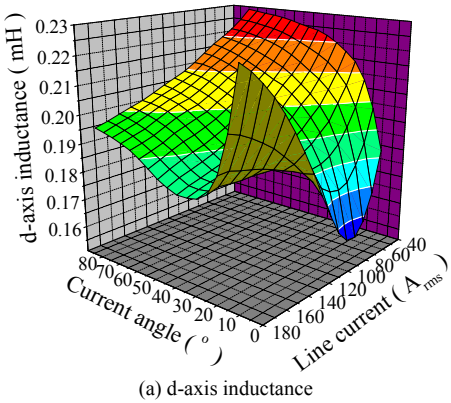

(a) d-axis inductance

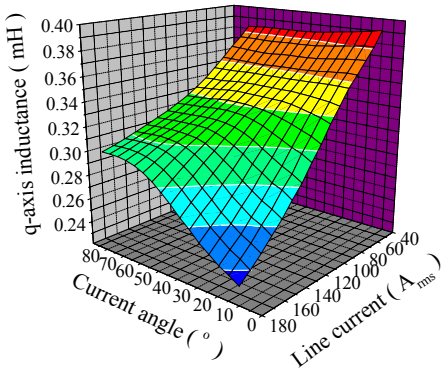

(b) q-axis inductance

Fig. 5. d- and q-axis inductance profile of 16-pole/24-slot model

IV. CHARACTERISTICS ANALYSIS

A. *d-q axis equivalent circuit analysis*

In order to calculate characteristics of IPMSM, d-q equivalent circuit analysis is employed. Equivalent circuit frame including iron loss are presented Fig. 6. The mathematical model of the equivalent circuits is given as follow equations. Iron loss is considered by equivalent resistance R_c, and the d- and q-axis voltages and effective torque equations are given by (4), (5) and (6), respectively. Where id and i_q are d- and q-axis component of armature current, i_{cd} and i_{cq} are d-and q-axis component of terminal voltage, R_a is armature winding resistance per phase, R_c is iron loss resistance, Ψ_a is flux linkage of permanent magnet per phase (rms value), L_d and L_q are d-and q-axis armature self inductance, and P_n is pole pair [3].

$$\begin{bmatrix} v_d \\ v_q \end{bmatrix} = R_a \begin{bmatrix} i_{od} \\ i_{oq} \end{bmatrix} + \left(1 + \frac{R_a}{R_c}\right) \begin{bmatrix} v_{od} \\ v_{oq} \end{bmatrix} + p \begin{bmatrix} L_d & 0 \\ 0 & L_q \end{bmatrix} \begin{bmatrix} i_{od} \\ i_{oq} \end{bmatrix} \tag{4}$$

$$\begin{bmatrix} v_{od} \\ v_{oq} \end{bmatrix} = \begin{bmatrix} 0 & -\omega L_q \\ \omega L_d & 0 \end{bmatrix} \begin{bmatrix} i_{od} \\ i_{oq} \end{bmatrix} + \begin{bmatrix} 0 \\ \omega \psi_a \end{bmatrix} \tag{5}$$

$$T = P_n \left\{ \psi_a i_{oq} + \left(L_d - L_q\right) i_{od} i_{oq} \right\} \tag{6}$$

B. *d- and q-axis inductance and saliency ratio*

The three models are analyzed by d-q axis equivalent circuit analysis. When the three models have same torque with same speed, variation of d- and q-axis inductance according to speed is calculated as shown Fig. 7. The variation of d- and q-axis inductance of three models is raised according to speed increasing. Although the aspect of d- and q-axis inductance variation is similar, saliency ratio of 16-pole/18-slot model has lower than other two models by t 40~50%. This result shows that 16-pole/18-slot model is weak to generate reluctance torque.

The 16-pole/18-slot model, however, 16-pole/18-slot which

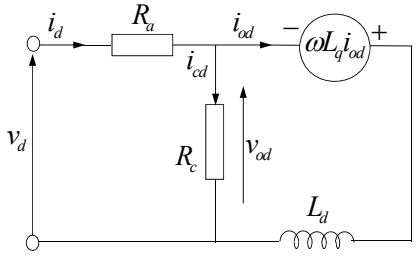

(a) d-axis equivalent circuits

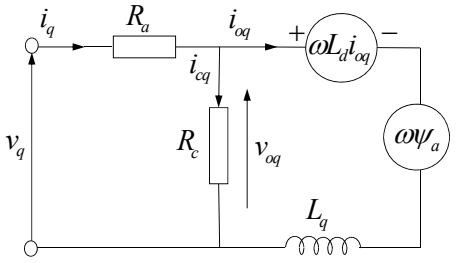

(b) q-axis equivalent circuits

Fig. 6. Equivalent circuit of IPMSM

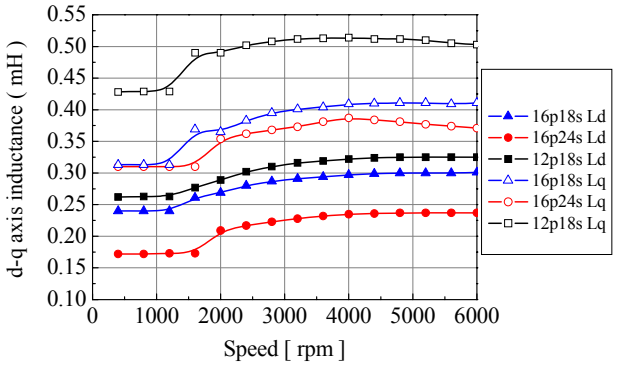

(a) d- and q-axis inductance

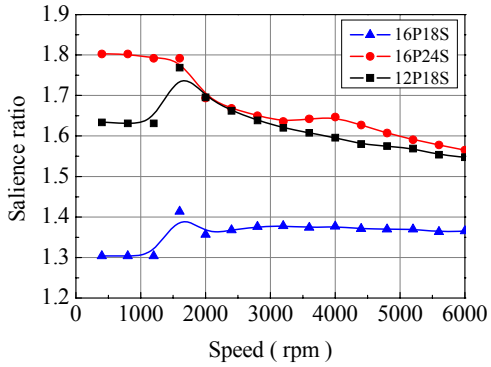

(b) Saliency ratio

Fig. 7. d- and q-axis inductance and saliency ratio according to speed

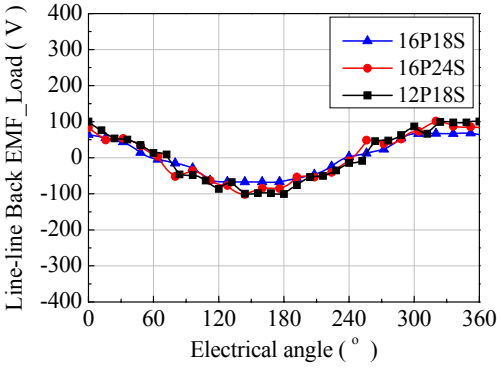

(a) 1200rpm

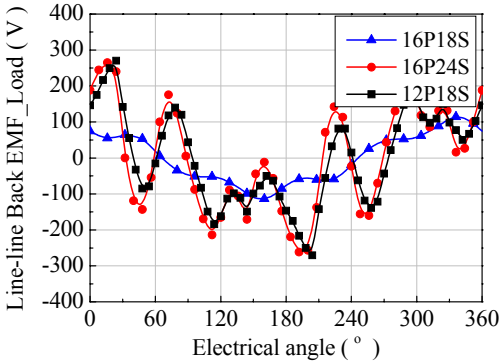

(a) 6000rpm

Fig. 8. Load back-EMF

TABLE IV
COMPARISON OF SALIENCY RATIO

Model	16-pole/18-slot	16-pole/24-slot	12-pole/18-slot
Saliency ratio @2000rpm	1.35	1.69	1.67
Saliency ratio @6000rpm	1.37	1.57	1.55

TABLE V
COMPARISON OF THD OF LOAD BACK-EMF

Model	16-pole/18-slot	16-pole/24-slot	12-pole/18-slot
THD of 1200rpm [%]	9.1	15.7	11.7
THD of 6000rpm [%]	18.9	106.4	81.4

has high winding factor. It can produce higher back-EMF, about 9% batter than the others. Therefore, line current for the rated torque is same with 16-pole/24-slot and 12-pole/18-slot model.

C. Load back-EMF

The flux weakening control is necessary to ensure wide speed range in the IPMSM [4]. In the low speed range controlled by MTPA, load back EMF has relatively sinusoidal shape. However the distortion of load back-EMF is increased at high speed due to d-axis magnetic force. High THD of back-EMF at load condition causes current harmonics and increases iron loss and eddy current loss in PM [5]. Fig. 8 (a) and (b) shows the back-EMF at load condition, 2000rpm and 6000rpm, respectively. The load back-EMF is calculated by FEA. The linkage flux at the load condition is computed for calculates load back-EMF and load back EMF is calculated using follow (7). Table IV shows THD of each waveform. The 16-pole/18-slot model is great advantage to drive high speed.

$$e_{load} = -\frac{d\lambda}{dt} \tag{7}$$

where e_{load} is load back-EMF and λ is linkage flux at load

D. Cogging torque and torque ripple

Cogging torque and torque ripple is important factor in the traction motor for HEV because most drivers are sensitive for vibration of vehicle. The cogging torque and torque ripple is related with vibration directly during EV mode. The EV mode is that HEV is driven by only traction motor. When the IPMSM is controlled by flux weakening control, generally it has apt to increase torque ripple. On the other hand, there is high cogging torque in IPMSM due to saturation partly. Fig. 9 shows cogging torque and torque profile at 6000rpm. The cogging torque is decreased as high as its frequency.

Frequency of cogging torque is determined by the least common multiple of pole and slot. The least common multiple of pole and slot for the 16-pole/18-slot model is 144 which is 8 times bigger than 16-pole/24-slot model. It is also 4 times bigger than 12-pole/18-slot model. Table VI shows the value of cogging toque and torque ripple about three models. This result shows the 16-pole/18-slot model has an advantage for vibration [6]. However, 16-pole/18-slot model is not guarantee vibration because there is the other vibration source exists which is normal direction force.

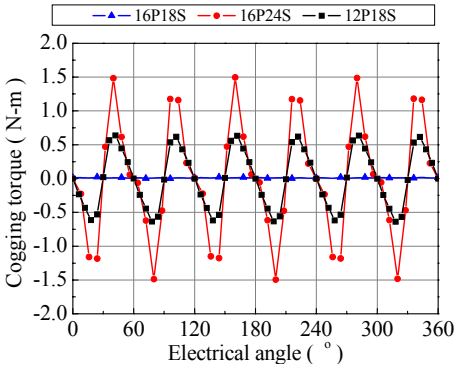

(a) Cogging torque

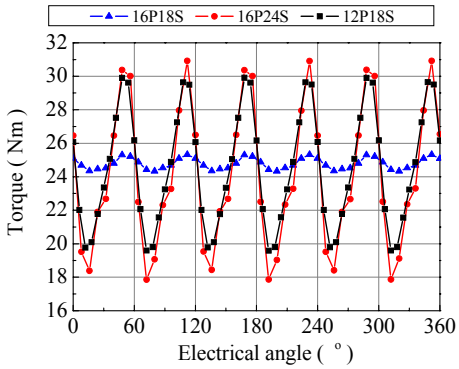

(b) Torque profile @6000rpm

Fig. 9. Cogging torque and torque profile

TABLE VI
COMPARISON OF THD OF NO-LOAD BACK-EMF

Model	16-pole/18-slot	16-pole/24-slot	12-pole/18-slot
Cogging torque [Nm]	0.02	2.99	1.28
Torque ripple @6000rpm [%]	4.0	54.4	42.2

E. Normal direction force

There is two kinds of force exist in the motor. One is tangential direction force which generates torque. The other is normal direction force. The normal direction force makes noise and vibration during motor driving. The aspect of normal direction force generation is different according to the number of Combination of the number of pole and slot.

Fig. 10 shows the mechanism of normal direction force generation for 16-pole/18-slot model which is computed by analytic method. It shows flux density and force for mechanical angle 0° to 180°. The flux distribution in air-gap of 16-pole/18-slot model is not symmetric each of the electrical periods as shown in Fig. 10 (a). Moreover, flux distribution in air-gap is completely different according to variation of ωt, where ω is angular velocity and t is time of input current which is flowed in armature winding. Fig. 10 (b) shows the flux density in the air-gap which are produced by both d-axis current and PM. It also shows composited flux density.

There is no tangential direction force which produces torque when the current is flowed in the motor only d-axis direction. Therefore, the composited flux density in air-gap which is

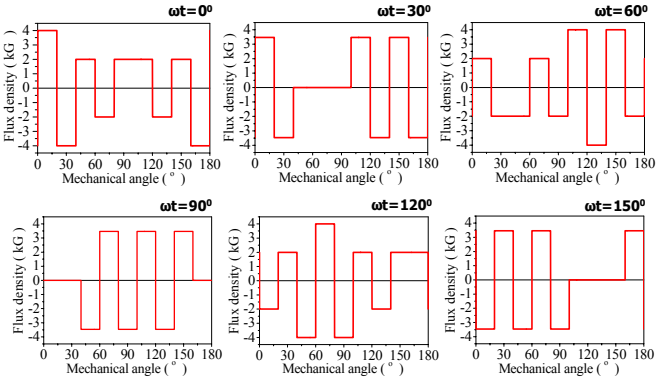

(a) Flux density in air-gap produced by armature winding

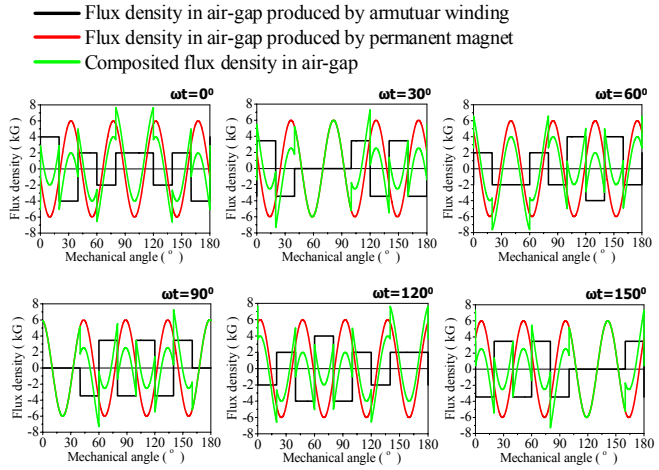

(b) Composition flux density in air-gap

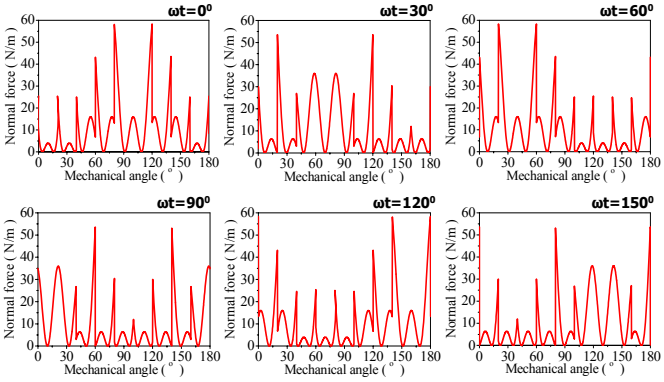

(c) Normal direction force distribution

Fig. 10. The mechanism of normal direction force generation for 16-pole/18-slot model

shown in Fig. 10 (b) is produces only normal direction force. According to the fact that the force is propositional to squire of flux density, normal direction force is calculated as shown in Fig. 10 (c). The normal direction force distribution of 16-pole/18-slot model is not symmetric each of the electrical periods. There is two or three maximum spot of normal direction force for the 0° to 180° mechanical angle. The maximum spot of normal direction force is moved according to ωt variation of input current.

The normal direction force distribution of 16-pole/18-slot model is different with the other models. Fig. 11 shows the normal direction force distribution of three models which is analyzed by FEM. The value of normal direction force is similar but its distribution is quite different. The normal direction force distribution of 16-pole/24-slot and 12-pole/18-slot model is symmetric each 45° and 60° which is single electrical period, respectively. However, normal direction force of 16-pole/18-slot model is concentrated two regions and it is rotated as moving the rotor. It causes the noise and vibration in the 16-pole/18-slot model larger than the others.

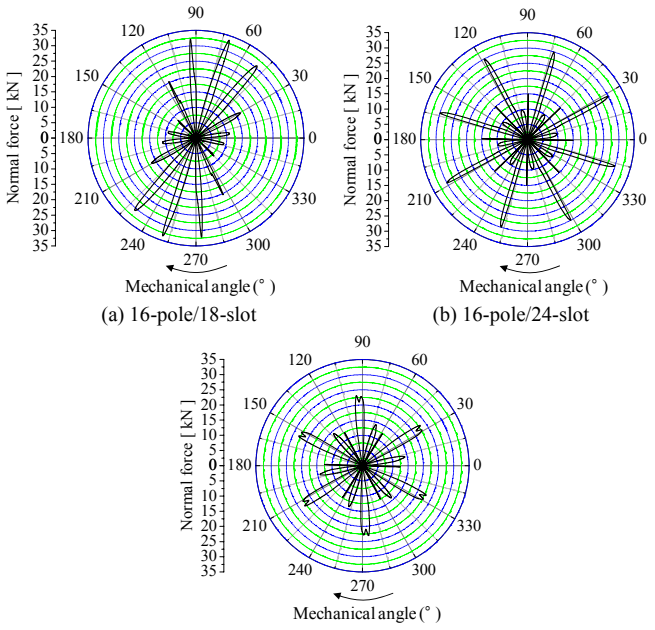

(a) 16-pole/18-slot (b) 16-pole/24-slot

(c) 12-pole/18-slot

Fig. 11. Normal direction force distribution

TABLE VII
COMPARISON OF GENERAL CHARACTERISTICS

	16-pole/18-slot	16-pole/24-slot	12-pole/18-slot
THD of Noload back-EMF	◎	○	○
Winding factor	◎	○	○
Saliency ratio	X	○	○
THD of Load back-EMF	◎	X	X
Cogging torque	◎	△	△
Torque ripple	◎	△	△
Normal direction force	X	○	○
Noise and vibration	X	○	○

◎: Excellent O: Good △: Not bad X: Bad

V. CONCLUSION

This paper deals with analysis and comparison of IPMSM which is applied to traction motor for HEV. Table VII shows the comparison of performance for 16-pole/18-slot, 16-pole/24-slot and 12-pole/18-slot model. It is determined by author. The 16-pole/18-slot model has low THD of back-EMF, cogging torque, torque ripple and high winding factor. This result shows that 16-pole/18-slot model is good agreement to apply traction motor in HEV. However, the normal direction force of 16-pole/18-slot model is not symmetric each of single electric periods. It causes noise and vibration during the motor driving. On the other hand, general characteristics of 16-pole/24-slot and 12-pole/18-slot model are lower than 16-pole/18-slot model but characteristics of noise and vibration is better than 16-pole/18-slot model. Therefore, 16-pole/24-slot and 12-pole/18-slot model is suitable combination of number of pole and slot to apply traction motor in HEV. If normal force of 16-pole/18-slot model is improved, it can be utilized to traction motor effectively.

REFERENCES

[1] Akira Nishio, Masahiro Hirano, Yoshiki Kato, Takayuki Irie and Tsutomu Baba, "Development of small size light weight and high power IPM motor for electric vehicle," Mitubishi Heavy Industries, Ltd. Technical Review, vol. 40, no. 5, 2003.

[2] Yoji Takeda, Nobuyuki Matsui, Shigeo Morimoto, Yukio Honda, "Design and control of interior permanent magnet synchronous reluctance motor," Ohmsa, 2001.

[3] Ji-Young Lee, Sang-Ho Lee, Geun-Ho Lee, Jung-Pyo Hong and Jin Hur, "Determination of Parameters Considering Magnetic Nonlinearity in an Interior Permanent Magnet Synchronous Motor," *IEEE Trans*., *Magn*., vol.42, no. 4, pp.1303-1306, April. 2006.

[4] Shigeo Morimoto, Yoji Takeda, Takao Hirasa and Katsunori Taniguchi, "Expansion of Operation limits for permanent magnet motor by current vector control considering inverter capacity," *IEEE Trans. Magn*., vol.26, no. 5, pp.866-871, Sept. 1990.

[5] Atsuhiko Yoneda, Takashi Miyoshi and Yasuo Shimizu, "Cogging torque target and design of motor for EPS," 2006 SAE World Congress, April, 2006.

[6] L. Ma, M. Sanada, S. Morimoto and Y. Takeda, "Iron loss predictin considering the rotational field and flux density harmonics in IPMSM and SynRM," *IEE proc.-Electr. Power*, Vol. 150, No. 6, Nov. 2003.

2007 Vehicle Power and Propulsion Conference

September 9 – 12, 2007

Wyndham (Sheraton Arlington) Hotel, DFW South Arlington, Texas, USA

- **Begin**
- **CD Help**
- **Preamble**
- **Technical Program**
- **Author Index**
- **Search**

IEEE Catalog Number: 07EX1461C

ISBN: 0-7803-9761-4

Co-Sponsored by:

Special Session 7: Electromechanical actuators for Vehicular Applications
Session Chair: Dr. Jin Hur
KETRI, South Korea
September 12, 2007
8:00 am – 9:00 am
Venue: SUPERBOWL – I

Characteristic Analysis and Comparison of IPMSM for HEV According to Pole and Slot Combination
Jae-Woo Jung, Jung-Pyo Hong and Young-Kyoun Kim[1]; *Hanyang Univ., [1]Korea Electronics Institute, S. Korea.*

Investigation on Characteristics and Optimal Shapes of Interior PM Synchronous Motor for Electric Vehicle Application
Sung-Il Kim, Jung-Pyo Hong and Jin Hur[1]; *Hanyang University, [1]Korea Electronics Technology Institute, S. Korea.*

Development of an Electric Driven Pump Unit for Electro-Hydraulic Power Steering of 42V Automobile
Se-hyun Rhyu, Yong-kyoun Kim, Jun-hyuk Choi, Jin Hur and Doo-hyung Lee[1]; *Korea Electronics Technology Institute, [1]Hyundai MOBIS, S. Korea.*

Post-break session: 10:30 am – 12:00 pm

Dynamic Control of Hybrid Energy Storage System for Mild HEV
Baek Haeng Lee, Dong Hyun Shin, Hyun Sik Song[1], Jin Beom Jeong[1], Hee Jun Kim and Byeong Woo Kim[2]; *Hanyang University, [1]Korea Automotive Technology Institute (KATECH), [2]Ulsan University, S. Korea*

The Development of Hybrid Electric Compressor Motor Drive System for HEV
Tae-Uk Jung, Sung-Ho Lee[1], Sung-Il Kim[2], Sung-Jun Park[3] and Jung-Pyo Hong[2]; *Kyungnam University, [1]Korea Institute of Industrial Technology, [2]Hanyang University, [3]Chonnam National University, S. Korea.*

Optimality and Reachability - Pseudo Boolean power Flows for multi-sourced Vehicle Topologies
George Kladis, John Economou, Antonios Tsourdos and Brian White*; Cranfield U.-Dept. of Aerospace Power and Sensors, USA.*